

AMERICAN UNIVERSITY OF BEIRUT

MICRO-PARTICLE INDOOR RESUSPENSION UNDER
PERIODIC AIRFLOWS: A NUMERICAL-ANALYTICAL
STUDY AND EXPERIMENTATIONS

by
MOHAMAD BASSEL ADNAN KAZZAZ

A thesis
submitted in partial fulfillment of the requirements
for the degree of Master of Engineering
to the Department of Mechanical Engineering
of the Faculty of Engineering and Architecture
at the American University of Beirut

Beirut, Lebanon
September 2016

AMERICAN UNIVERSITY OF BEIRUT

MICRO-PARTICLE INDOOR RESUSPENSION UNDER
PERIODIC AIRFLOWS: A NUMERICAL-ANALYTICAL
STUDY AND EXPERIMENTATIONS

by
MOHAMAD BASSEL ADNAN KAZZAZ

Approved by:

Prof. Kamel Abou Ghali, PhD, Professor
Department of Mechanical Engineering


Advisor

Prof. Nesreen Ghaddar, PhD, Professor
Department of Mechanical Engineering


Co-Advisor

Prof. Mohammad Ahmad, PhD, Professor
Department of Chemical and Petroleum Engineering


Member of Committee

Date of thesis defense: Friday September 9, 2016

AMERICAN UNIVERSITY OF BEIRUT

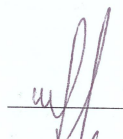
THESIS, DISSERTATION, PROJECT RELEASE FORM

Student Name: Kazzaz Mohamad Bassel Adnan
Last First Middle

Master's Thesis Master's Project Doctoral Dissertation

I authorize the American University of Beirut to: (a) reproduce hard or electronic copies of my thesis, dissertation, or project; (b) include such copies in the archives and digital repositories of the University; and (c) make freely available such copies to third parties for research or educational purposes.

I authorize the American University of Beirut, **three years after the date of submitting my thesis, dissertation, or project**, to: (a) reproduce hard or electronic copies of it; (b) include such copies in the archives and digital repositories of the University; and (c) make freely available such copies to third parties for research or educational purposes.


Signature

Monday, September 19, 2016
Date

ACKNOWLEDGEMENTS

I would like to express my deepest gratitude to my thesis adviser Prof. Kamel Abou Ghali for his advisory, guidance and patience through my graduate study.

I would also like to thank Prof. Nesreen Ghaddar for her recommendations, thoughtful ideas and help in completing this work.

Special thanks to Prof. Mohammad Ahmad for being a member of my thesis committee.

I would also like to thank Dr. Carine Habchi for her extensive and zealous aid throughout the thesis.

I would also like to show deep gratitude and appreciation to my family members and friends for their support throughout the past years.

AN ABSTRACT OF THE THESIS OF

Mohamad Bassel Adnan Kazzaz for Master of Engineering
Major: Mechanical Engineering

Title: Micro-Particle Indoor Resuspension Under Periodic Airflows: A Numerical-Analytical Study And Experimentations

As particles may pose a threat to people during breathing close to surfaces, understanding and identifying the mechanisms by which these particles detach help in taking preventive measures during cleaning and dusting processes of surfaces, and in the selection and operation of ventilation systems when particles are airborne. This work presents a numerical–analytical coupled model to examine resuspension under the effect of oscillatory flows, taking into account the probabilistic approach of resuspension occurrence due to turbulent bursts for different particle diameters and surface roughness. The results of the model were validated with experiments conducted for flows alternating between constant blowing and suction for different flow velocities and frequencies.

A parametric study using the validated model was conducted to study the particle detachment phenomenon under sinusoidal flows similar to human breathing flows under a variety of respiration velocities and rates, particle diameters and surfaces. Results showed that micro-particles of relatively high diameters pose a considerable threat over surfaces in indoor environment. The occurrence of resuspension is highly influenced by surface type and roughness. Parquet flooring was found to cause the resuspension of approximately 98% of 80 micrometer lead particles compared to 64.5% of the same particles over marble flooring at certain locations under the effect of normal breathing. Therefore, besides dust removal methods, the choice of flooring material is an essential preventive measure to reduce indoor particle resuspension.

CONTENTS

ACKNOWLEDGEMENTS	V
ABSTRACT	VI
LIST OF NOMENCLATURE	IX
LIST OF ILLUSTRATIONS	XI
LIST OF TABLES	XII

Chapter

I. INTRODUCTION	1
II. PROBLEM DESCRIPTION	4
III. METHODOLOGY	5
A. Numerical Methodology	5
B. Analytical Methodology	7
C. Experimental Methodology	9
1. Particle Seeding	10
2. Periodic Flow Generation	12
3. Resuspension Set-Up	14
4. Particle Detachment Quantification	16

IV. RESULTS AND DISCUSSION	18
A. Experimental Validation	18
B. Parametric Study	28
VI. CONCLUSION	37
BIBLIOGRAPHY	40

LIST OF NOMENCLATURE

Keywords: indoor resuspension, detachment fractions, square flows, sinusoidal flows, breathing, human exposure.

Nomenclature

Symbols

- D_F : boolean state of black pixel
- C : Cunningham factor to account for the slip effect on the drag force
- CFD : computational fluid dynamics
- F_B : measured detachment fraction
- d_p : particle diameter
- $F_{ad,JKR}$: adhesive force modeled by the JKR theory
- F_B : fraction of black pixels
- LES : Large eddy simulation
- N_B : number of black pixels
- N_T : total number of pixels in an image
- q_{avg} : average volumetric flow rate
- RSM : Reynolds stress model
- t : time
- u : stream wise velocity
- \bar{u} : mean velocity
- u' : fluctuating velocity
- u^* : friction velocity
- u^+ : normalized velocity
- u_t : stream component of U_t
- U_t : magnitude of the velocity vector at the particle center parallel to the wall

UDF : user-defined function
 v : respiratory flow velocity
 v_{max} : maximum respiratory flow velocity
 w : transverse velocity
 w_t : transverse component of U_t
 y : distance from the wall

Greek symbols

τ_w : wall shear stress
 ρ : fluid density
 ν : fluid kinematic viscosity
 ζ : randomly distributed number following the Gaussian distribution

ILLUSTRATIONS

Figure	Page
1: Top view of the resuspension setup under study (a) flow nozzle (b) seeded surface (c) oscillatory flow graph.....	4
2: Schematic representation of particle seeding setup.....	11
3: Oscillatory flow system design.....	14
4: Schematic drawing of the experimental setup under the microscope.....	15
5: Experimentally measured flow profile compared to the theoretical flow profile.....	19
6: CFD mesh treatment: (a) 3D view (b) Frontal view and (c) Cross-sectional side view.....	20
7: Shear stress variations over the region surrounding the flow outlet.....	21
8: Detachment fraction variations for particles of 49 μm at flow frequencies of 0.5Hz and 0.25Hz for flow velocities of (a) 2.5m/s (b) 3.5m/s.....	23
9: Detachment fraction variations for particles of 82.5 μm at flow frequencies of 0.5Hz and 0.25Hz for flow velocities of (a) 1.5m/s (b) 2.5m/s (c) 3.5m/s.....	24
10: Shear stresses during a blowing phase between 0 and 1s and a suction phase between 1 and 2s.....	26
11: Shear stress variation over the surface under the influence of normal breathing.....	30
12: Detachment fraction variations for (a) lead (b) nickel particles of sizes 25 μm and 80 μm	33
13: Detachment fraction variations for (a) lead and (b) nickel particles of size 80 μm under different flooring materials.....	36

TABLES

Table	Page
1 : Seeding densities for every particle diameter	12
2: Boundary conditions used for the setup in the parametric study	31
3: Particle properties used in the parametric study	31
4: Substrate / Flooring properties used in the parametric study	31

CHAPTER I

INTRODUCTION

Particle resuspension is the physical phenomenon known by the particles' detachment from a surface followed by its re-entrainment in the air [1]. Particle resuspension enters in the formulae of human health and indoor air quality due to the hazardous materials carried by these particles [2]. Indoor environments contain a variety of dust particles, which can arise from both indoor and outdoor sources. Smoking and cooking were found to be the two main indoor sources for particles, contributing to dust elements as potassium, aluminum, iron, chlorine and calcium [3,4]. On the other hand, more than half of the indoor particles were found to come from outdoor sources such as heavy metals (Lead, Nickel, Zinc, Copper and Lithium) from vehicles' exhaust particles and pesticides present due to indoor/outdoor air exchange [3,5-9]. Indoor particle sizes range from fractions of a micrometer up to few millimeters; however particles below the size of a 100 μm are taken into human exposure risk assessments [10]. Previous studies have shown that particle deposition occurs abundantly on living room floors due to the high daily activity in such spaces [11]. Mattresses were found to be reservoirs of dust particles and powder, which may be transferred through the house and to other floors when stuck to feet of residents or hands of small infants [10,11].

Predicting resuspension is a crucial concern to human health, as these particles are subject to inhalation and may cause respiratory allergies and trigger the immune system [11-13]. Accumulation of depositions along the respiratory tract may be a major issue to consider when observing indoor resuspension. In an indoor ventilated

environment, it was reported that during a single inhalation, an average of 0.0014% of the total mass of pollutants inhaled per person was transferred to the human body [14], which poses a serious health risk. Particles resuspending from surfaces are capable of carrying allergens such as pet dander, birch pollen and house dust mite [11,15-17].

Dust reservoirs disturbed by human activity release carrier particles leading to occupant inhalation exposure [15]. Human activities such as walking, dusting, vacuuming have been previously identified to cause resuspension in indoor environments [18]. Other mechanisms, which are not common but might be capable of initiating detachment and resuspension, involve breathing close to surfaces seeded with particles [19]. Respiration is a type of oscillatory flows, which might be capable of causing resuspension in cases of crawling babies on floors, prostration position during praying and sleeping on a pillow where the seeded surfaces are in the vicinity of nasal and oral cavities [19].

Particle resuspension under periodic or oscillatory flows has not been examined extensively. Respiration, and despite its low velocity, has a transient nature of accelerating and decelerating alternations during both inhalation and exhalation [20]. Velocity fluctuations occurring due to turbulent bursts in the hydrodynamic boundary layer over surfaces contribute to resuspension occurrence at lower flow velocities [21].

A recent model developed by Habchi et al. [22] investigated resuspension under the effect of transient flows through an analytical model coupled with a numerical model. It predicted resuspension in a probabilistic manner, accounting for variations in surface shear stresses due to turbulent bursts occurrence, surface roughness and particle dimensions. The model was validated with the published experimental results of

Ibrahim et al. for accelerating flows [23]. However it would be of interest to extend the applicability of their transient model to more complex transient flows such as periodic flows with suction and blowing.

Oscillatory flows are interesting since they exist in several natural mechanisms, where the flow pattern of human breathing in particular is considered to be one of the periodic flows [20,24]. In addition to flow velocity and acceleration, periodic flows introduce a new parameter that needs to be considered in resuspension mechanisms which is the flow frequency [20].

This study investigates resuspension under the effect of oscillatory flows. The methodology involves using the coupled analytical and Computational Fluid Dynamics (CFD) model of Habchi et al. [22]. An experimental setup is developed to test resuspension of particles for sizes and conditions present in houses and indoor environments. Experimental work is performed to validate the developed model accuracy in predicting transient particle resuspension under the influence of oscillatory flows. This is followed by a parametric study to assess the effect of different factors such as flow velocity, frequency, particle size and surface type in on resuspension.

CHAPTER II

PROBLEM DESCRIPTION

To study the resuspension phenomenon, particles of different diameters are seeded over surfaces, which in turn are subjected to periodic flows from a flow source close to the surface as shown in **Fig. 1(a)** and **(b)**. The velocity and frequency of the oscillatory flow are varied following the general flow profile presented in **Fig. 1(c)**. The effect of the particle diameter, flow velocity and frequency on the detachment rates and fractions are examined.

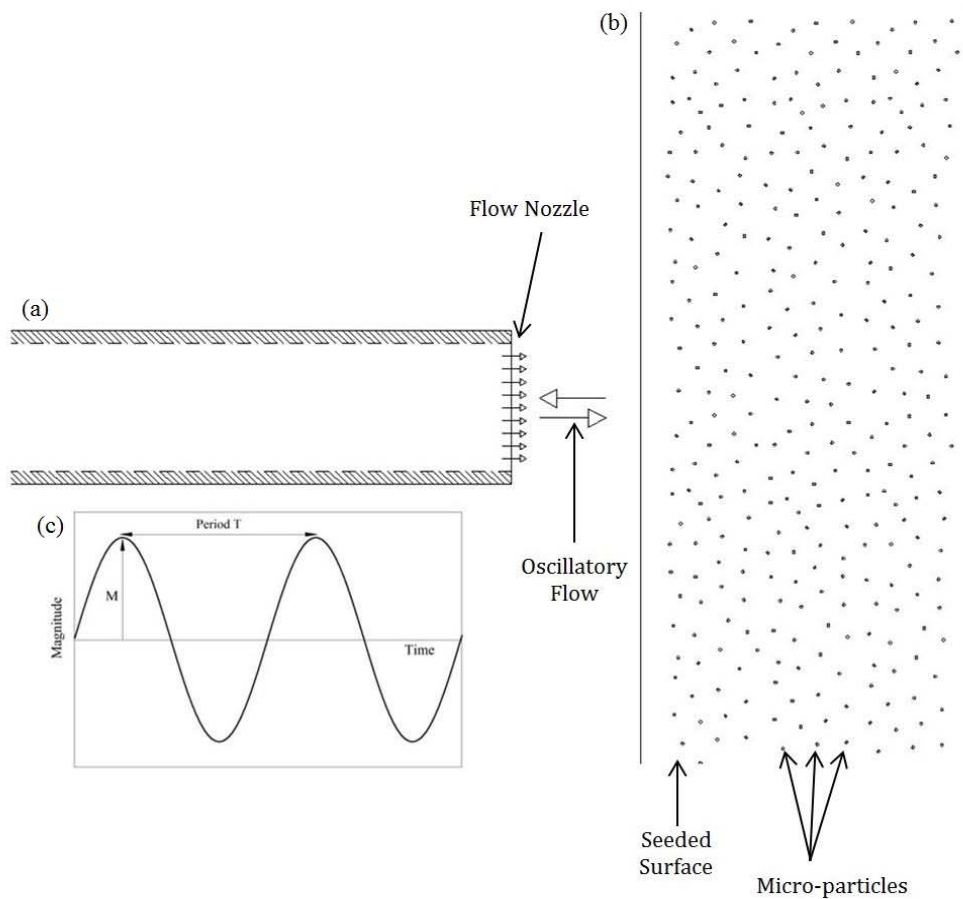


Figure 1: Top view of the resuspension setup under study (a) flow nozzle (b) seeded surface (c) oscillatory flow graph

CHAPTER III

METHODOLOGY

To achieve the goals of predicting resuspension under the influence of periodic flows, it is essential to resolve the velocity field surrounding the particle in the viscous sub layer. Computing the velocity components in this thin layer requires the determination of the shear stress distribution over the surface of interest. Since complex physics is involved in the case of transient boundary layer flow development, computational fluid dynamics (CFD) simulations were performed. The shear stresses map obtained from CFD simulations was then coupled with the analytical model of Habchi et al. [22] to obtain the mean and fluctuating velocities taking into account the probabilistic behavior of turbulent bursts within the flow boundary layer. Both mean and fluctuating velocities contribute to the hydrodynamic forces and moments acting on the particle, which determine the occurrence and mode of resuspension. Numerical-Analytical results were validated with experiments conducted under variable conditions. Moreover, a parametric study was performed to investigate resuspension under variable conditions of low velocity and frequency.

A. Numerical Methodology

The CFD software ANSYS Fluent [25] was used to resolve for the shear stress map over the surface of interest. The computational domain geometry consisted of a surface placed inside a box with the upper and frontal faces exposed to atmospheric conditions and was subjected to a parallel flow from a source generating a periodic flow

facing the surface. The surface was discretized into small squares in order to be capable of computing and monitoring the shear stress distribution as function of position and time close to the surface. The geometry was meshed into unstructured tetrahedral elements. To resolve for the velocity field within the viscous sub layer, mesh adaptation was performed to insure that the dimensionless wall distance was in the range of $1 < y^+ < 5$. To ensure this condition, the surface of interest was treated with the appropriate face sizing and inflation at a growth rate of 1.2.

Flow turbulence can be fully captured by Direct Numerical Simulation (DNS) consisting of solving directly for the Navier-Stokes equations but the computational time it requires is extremely large [25]. The CFD model should accurately resolve for the velocity field within the hydrodynamic boundary layer, thus it is crucial to select the appropriate turbulence model accounting for the anisotropic turbulence effects in this region. The $k - \epsilon$ and $k - \omega$ turbulence models are not suitable for the current application since they assume isotropic fluctuating velocities in all directions near the surface. Moreover, the Large Eddy Simulation (LES) method uses the DNS to resolve for large eddies without accounting for small eddies which are dominant near the surface, thus requiring higher computational cost without improving the model predictions accuracy. On the other hand, the Reynolds – Stress Model (RSM) accounts for turbulence anisotropies near surfaces at reasonable computational cost which renders accurate results for the fluctuating velocities components. Enhanced wall treatment was selected to capture turbulent bursts effect within the different boundary sub-layers.

The PRESTO! scheme was used to solve for pressure, while the SIMPLE algorithm was chosen for the pressure-velocity coupling. The Second Order Upwind

scheme was picked to resolve for the rest of the spatial elements as energy, momentum, Reynolds stresses, and turbulent energy and dissipation rate.

The characteristics of periodic flow are defined in a user-defined function (UDF) where the profile, frequency and magnitude of the flow are set for every simulation case. For every profile of airflow, the effect of the velocity magnitude and frequency was examined through the obtained shear stress map. Moreover, a comparison was done to study the effect of the flow profile at fixed conditions of air velocity magnitudes and frequencies.

B. Analytical Methodology

Particle resuspension prediction is based on coupling the numerical results of the shear stresses obtained through computational fluid dynamics with the analytical model developed by Habchi et al. [22] using MATLAB software [26]. This approach includes finding stream wise velocity, in terms of the dimensionless wall distance y^+ according to Soltani and Ahmadi's correlation [27] and using a stochastic approach to model the probabilistic turbulence behavior as shown in Eq. (1):

$$u^+ = \bar{u}^+ + u'^+ = \bar{u}^+ + \zeta u'^+_{rms} = y^+ + \zeta(0.25y^+ + 0.0325y^{+2}) \quad (1)$$

where, u^+ is the normalized stream wise velocity, \bar{u}^+ is the normalized mean velocity, u'^+ is the normalized fluctuating velocity, u'^+_{rms} is the normalized root mean square fluctuating velocity, and ζ is a random number following the Gaussian distribution. Since y^+ can be expressed in terms of the friction velocity u^* , the distance from the wall y , and the kinematic viscosity of the fluid ν , the normalized stream wise velocity can be given by:

$$u^+ = \frac{u^* y}{\nu} + \zeta \left(0.25 \frac{u^* y}{\nu} + 0.0325 \left(\frac{u^* y}{\nu} \right)^2 \right) \quad (2)$$

The friction velocity u^* is defined as the square root of the shear stress τ_w over the fluid density ρ . Due to presence of eddies within the viscous sub layer, deviations occur in the flow dividing the total flow into two components, the stream velocity component u and the transverse velocity w , where w^+ (Normalized Transverse Velocity) is equivalent to $0.54u^+$ (Normalized Stream Velocity) according to Ahmadi and Soltani [27]. Therefore the magnitude of total flow velocity parallel to the surface U_t is given by Eq. (3) as follows:

$$U_t = \sqrt{u^2 + w^2} = u^* \sqrt{u^{+2} + w^{+2}} = u^* \sqrt{u^{+2} + 0.2916 u^{+2}} = u^* \sqrt{1.2916 u^{+2}} \quad (3)$$

Using the correlation in Eq. (2), U_t can be presented in the form of Eq. (4):

$$U_t = \sqrt{\frac{1.2916 \tau_w u^{+2}}{\rho}} = 1.13648 \frac{\tau_w}{\mu} + 0.28412 \zeta \frac{\tau_w}{\mu} + 0.0369 \zeta^2 \frac{\tau_w^{1.5} y^2}{\mu^2} \quad (4)$$

Using the total velocity U_t , the drag force [23], the lift force [28] and the surface stress moment [22] acting on the particle can be computed. On the other hand, the force of adhesion between the particle and the surface can be calculated from

$$F_{ad} = C * F_{ad,JKR} \quad (5)$$

where, C is a roughness ratio modeled by Dunn [29] and $F_{ad,JKR}$ is the force of adhesion according to JKR theory [30].

The computed forces and moments are involved in three different modes of resuspension as observed by Ibrahim et al. [23]: rolling, sliding and direct liftoff. The resuspension mode depends on the satisfaction of one of the force balance (sliding or liftoff) or moment balance (rolling) rupture conditions presented by Ibrahim et al. in three inequalities [23].

According to Habchi's model [22], the presence of a probabilistic behavior when considering resuspension is mainly due to three factors. At any position and time, turbulent bursts in the hydrodynamic layer follow a Gaussian profile. Moreover, surface roughness and particle diameters vary according to independent distribution functions. Thus, probabilistic behavior of resuspension is taken into account by multiplying the probability of turbulent bursts occurrence with the probability of surface roughness and particle diameter distributions [22]. The total probability of resuspension over the considered sample P_r at a time t can be given by:

$$P_r(t) = \sum_{j=1}^m \sum_{i=1}^n p_j * p_i * p_{b,ijt}(t) \quad (6)$$

where, p_j and p_i represent the probabilistic effects of particle diameter and surface roughness distributions on $P_r(t)$, and $p_{b,ijt}$ the resuspension probability driven by the stochastic behavior of turbulent bursts occurrence for a certain values of particle diameter and surface roughness at time t .

C. Experimental Methodology

An experimental setup generating periodic flows was constructed to test for resuspension under variable conditions. Experiments were conducted to validate the transient resuspension model under the influence of square signaled flows of blowing and suction involving variable frequencies and flow velocities.

Commercially available "White Polyethylene Micro-particles" were obtained from Cospheric LLC (Micro-particles supplier) with sizes of $49\mu\text{m} (\pm 4\mu\text{m})$ and $82.5\mu\text{m} (\pm 6\mu\text{m})$ and a density of 1.00 g/cm^3 quoted by the manufacturer. Microscopic glass slides of size $25.4\text{ mm width} \times 76.2\text{ mm length} \times 1\text{ mm thickness}$ with an average

surface roughness of 4 μm ($\pm 0.4 \mu\text{m}$), measured using a TR220 profilometer, were used as sample surfaces. All surfaces prior the particle seeding, were immersed in a solution of Decon-90 solution for two hours, then rinsed thoroughly with distilled water and left to dry by evaporation in a glassware drying oven at 65°C. All particle seeding procedures and experiments were conducted at a temperature of 28°C ($\pm 0.8^\circ\text{C}$) and a relative humidity of 35% ($\pm 3\%$).

1. Particle Seeding

To ensure gravitational settling of the particles over the surfaces, seeding was carried in a Plexiglas cubic enclosure as shown in **Fig. 2** (0.3m \times 0.3m \times 0.5m). The samples were evenly distributed covering all regions over the floor of the seeding chamber and the microspheres were sequentially released into the funnel and through the airflow passing in the particle injection tube detailed in **Fig. 2**. The airflow was dehumidified through silica filters (Parker Balston) and cleaned from micro and nanoparticles through a filter (Hepa-Cap 75).

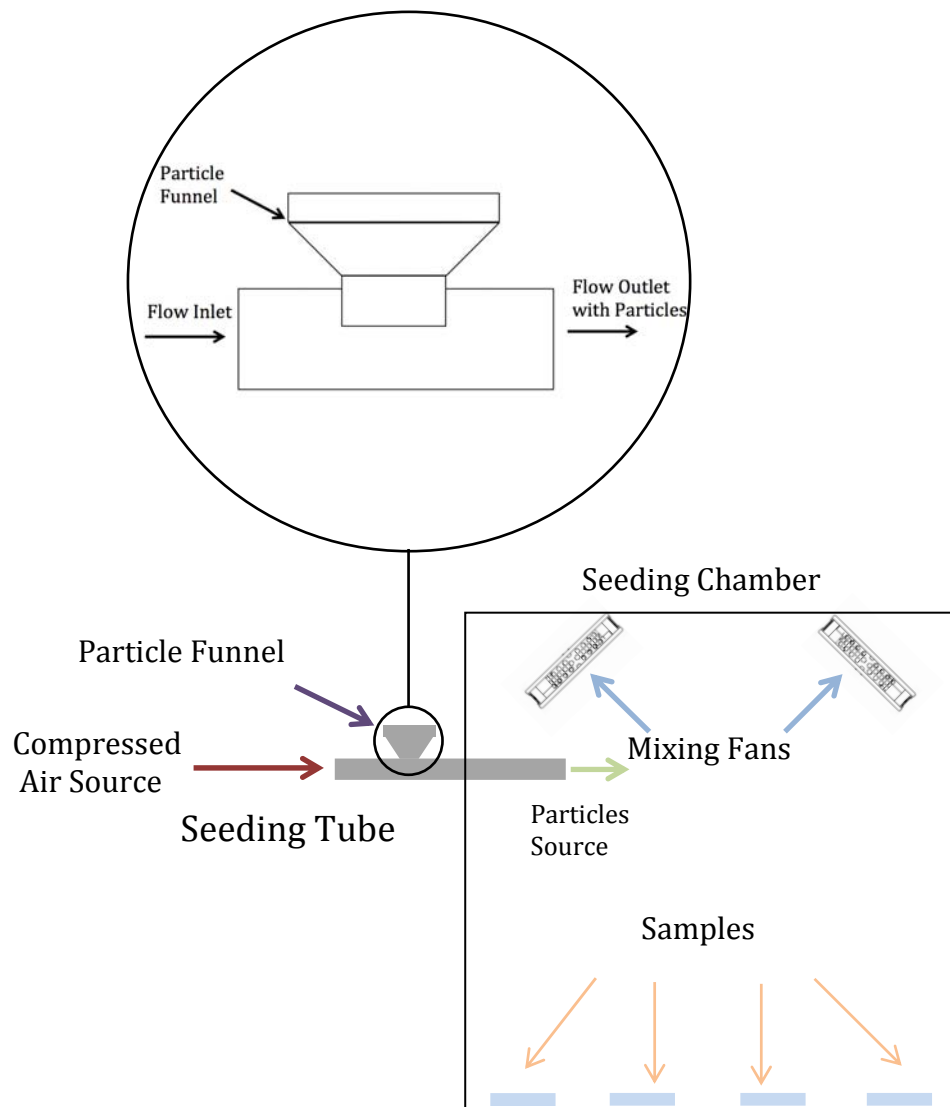


Figure 2: Schematic representation of particle seeding setup

To achieve a mono-dispersive distribution of particles over the sample surfaces, two small fans were left to run for inside the chamber to create a homogenizing effect. The chamber was left sealed for a sufficient time to allow the gravitational settling of the particles to occur over the sample surfaces. To determine the seeding mass of micro particles required in achieving repeatability for each particle size, the coverage area of

the particles was quantified. Following this experimental procedure, an average particle coverage area of 30% was found to be suitable to avoid agglomerations and ensure monolayer dispersion. Seeding procedures were repeated three times for each particle diameter, where several counting measurements were done on different regions of each sample to ensure a relatively uniform coverage area of particles over the different regions of the seeding chamber. The seeded masses along with the obtained average particle densities and coverage area of the micro particles per unit area are presented in Table. 1.

Table 1 : Seeding densities for every particle diameter

Particle Diameter	Mass of Particles Injected	Chosen Percentage Coverage Area	Average Concentration	Standard Deviation
49 μm	0.5705g (\pm 0.01mg)	20%	106.1 particles/mm ²	6.11
82.5 μm	0.8132g (\pm 0.01mg)	20%	37.41 particles/mm ²	3.29

To ensure a monolayer distribution of the particles, sample surfaces were examined under a microscope (Olympus SZX10) which can give a three dimensional view of the seeded surfaces with a magnification ratio of 1.5X. The microscope uses an inverted lighting source, which illuminates and displays the different layers of the sample. The samples were examined to ensure that no particles were deposited beyond the first layer of seeding.

2. Periodic Flow Generation

Delivering a set of transient flows through the experiment requires a system capable of generating flows of varying profiles, frequencies and magnitudes. **Fig.3**

shows a diagram of the experimental setup for the resuspension experiment. The particles seeded over the surface are subjected to square signaled flows of periodic blowing and suction phases.

To deliver square flows over the surface at (13), the system functions as follows. A discharge flow is supplied to the system at (1) from a compressor pump (General Electric GAST), while a vacuum pump (General Electric G588DX) at (4) creates a suction flow through the system. During a discharge phase, the 3-way valve at (7) directs the compressed air from (1) towards the seeded surface at (13), while the suction flow is switched to withdraw air from external conditions at (5a). On the other hand, during a suction phase, the 3-way valve at (7) switches the suction flow to be withdrawn from the surface at (13) towards the pump at (4), while compressed air leaves from the outlet vent at (2a).

A flow meter (TSI 41211) at (9) measures the volumetric flow rate of the suction and discharge flows while sending a feedback signal to two proportional valves (OMEGA PV104-10), where the flow passing through (3 & 6) is controlled through adjusting the orifices of the valves. A Data Acquisition Card (National Instruments NI-myDAQ) was used to deliver periodic digital signals and measure the analog feedback signals.

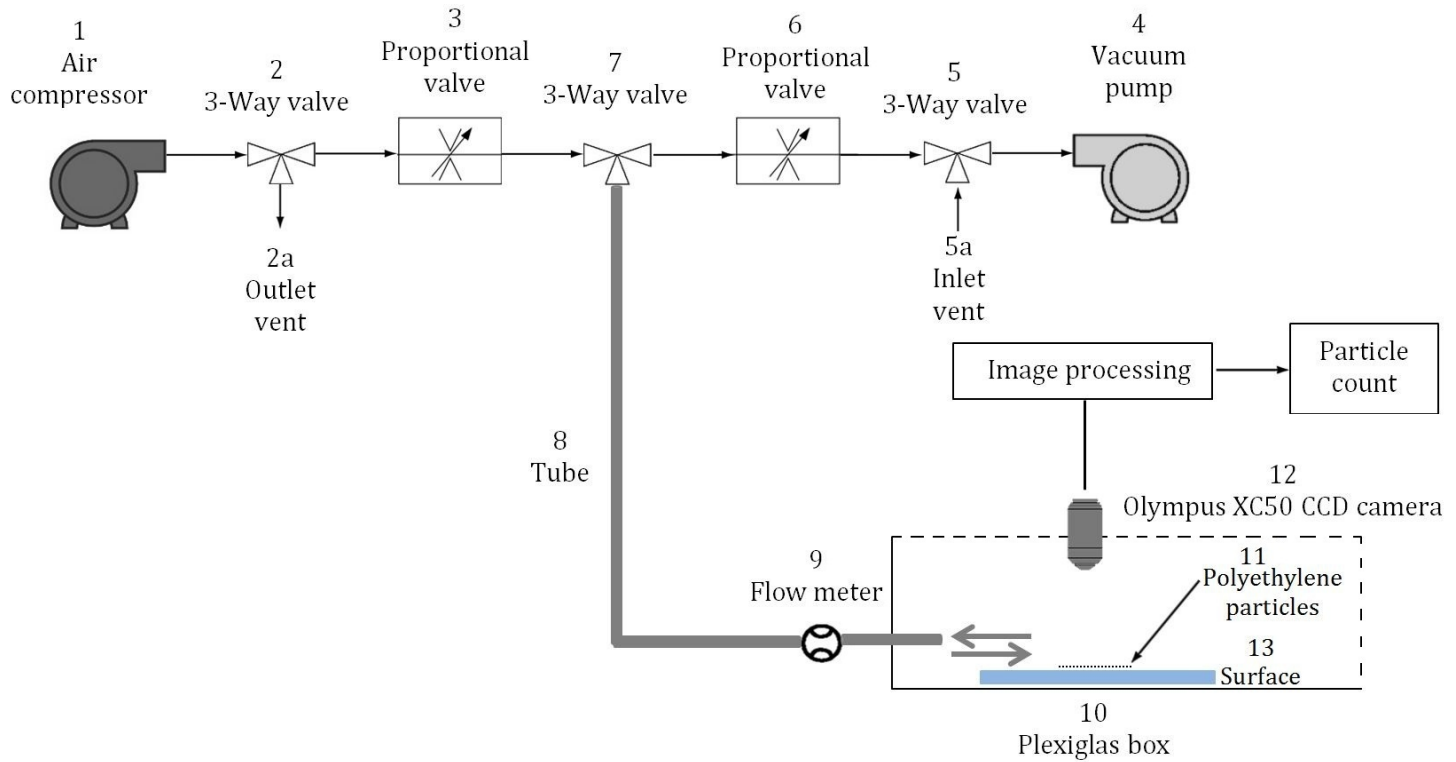


Figure 3: Oscillatory flow system design

3. Resuspension Set-Up

Experiments were conducted inside a Plexiglas enclosure under the microscope, where seeded surfaces were subjected to parallel periodic flows from the outlet of the transient flow generating system. The Plexiglas box (20 cm × 20 cm × 4 cm) shown in **Fig. 4** at (10), was used to prevent undesirable external flows from interfering through the experiment. The topside of the box was open to allow the vertical movement of the microscope objective over the samples. On the other hand, the frontal side facing the outlet of the transient airflow system was removed allowing a continuous airflow over the surface.

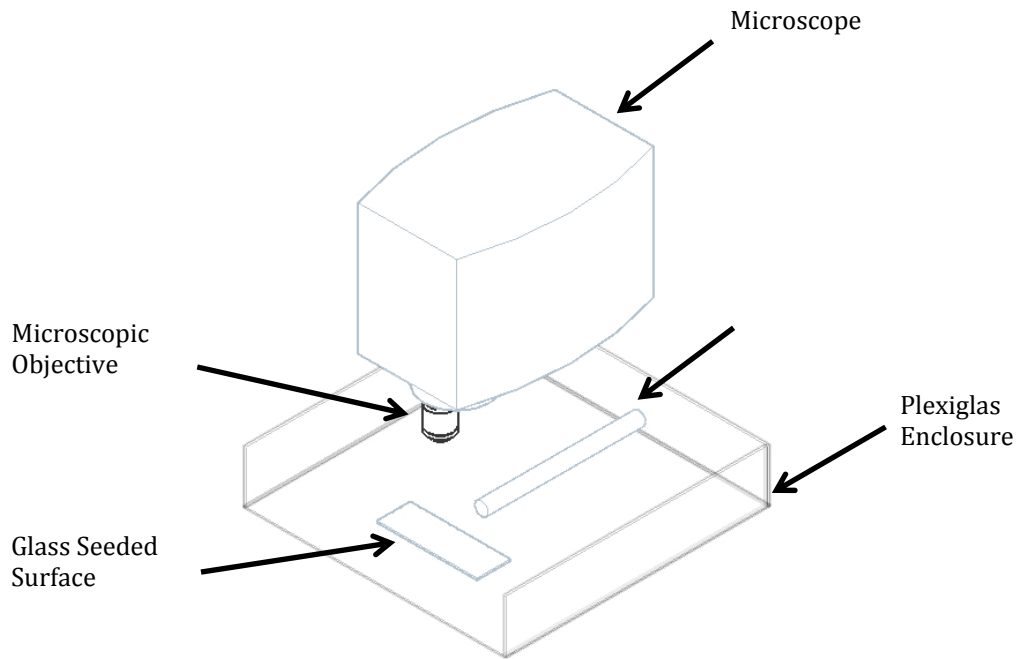


Figure 4: Schematic drawing of the experimental setup under the microscope

The outlet of the flow generating system is a tube with an inner diameter of 1cm and placed at a distance of 1cm from the frontal edge of the sample where the flow exhibits the highest shear stresses as will be shown in section 4.1. The Plexiglas box carrying the seeded surface and the tube were firmly fixed to the stage of the microscope, where the outlet tube of the flow was clamped tight in position to the bottom side of the Plexiglas, while small engraves secured seeded sample in place on the set up to ensure repeatability throughout the carried experiments.

The experiments were conducted under a microscope (Olympus BX41M-LED) with a magnification objective of 5× and equipped with a 5MP camera (Olympus XC50) having an image resolution of 2576×1932 pixel CCD with a frame rate of 22.5 fps. The lens of the microscope was fixed at a height of 5cm from the sample surface, while the scan area viewed by the microscope was $1.2\text{mm} \times 1\text{mm}$, located at a distance

of 1 cm from the center of airflow outlet. To ensure the same region was considered in each experiment, measurements were taken using the automated stage of the microscope from the bottom left corner of each sample to the focus area located near the lower edge of the horizontal center of the sample. The considered region under the microscope is the most influenced area by the generated flow compared to other locations over the sample, thus the highest detachment rates are expected over this region.

Periodic square flows of blowing and suction were considered for the experiments, where particle detachment was assessed under the effect of two main airflow characteristics, which are the flow velocity and frequency, and one main particle characteristic, which is the particle diameter. Validation is done for airflow velocities of 1.5 m/s, 2.5m/s and 3.5m/s at both frequencies of 0.5 Hz and 0.25 Hz, and two particle diameters (49 μm and 82.5 μm) of polyethylene microspheres.

4. Particle Detachment Quantification

Digital image processing was applied to track detachment fractions throughout the experiments, where a computer vision program was developed using the “LabVIEW- Vision” and “IMAQ” software for particle size analysis [33]. This method of full scan inspection of particle sizes and shapes was previously used by Liao et al. [34], where particle size distributions measurements rendered a precision of around $\pm 1\%$. Videos of the experiments were recorded, which were synchronized with the flow generation system. Binary images of the captured region were taken throughout the cycles, where areas covered by particles appeared in black, while empty regions appeared in white. Measuring the area covered by particles was done by quantifying the

number of black pixels through the vision program in the image denoted by N_B given in Eq. (7):

$$N_B = \sum_0^{P_x} \sum_0^{P_y} B(x,y) \quad (7)$$

Where, $B(x,y)$ is:

$$B(x,y) = \begin{cases} 0, & \text{if the pixel is white} \\ 1, & \text{if the pixel is black} \end{cases}$$

where, P_x represents the number of pixel columns of the image, P_y represents the number of pixel rows, x represents the abscissa of the pixel and y represents the ordinate of the pixel in the image. The number of black pixels N_B is divided by the total number of pixels in the image N_T to obtain the fraction of black pixels F_B in the image as presented in Eq. (8):

$$F_B = \frac{N_B}{N_T} \quad (8)$$

where, the total number of pixels N_T in an image is given by:

$$N_T = P_x \times P_y \quad (9)$$

where given the used microscope Olympus XC50 camera of resolution of 2576×1932 pixel, a total of 4,976,832 pixels is obtained which is approximately at total of 5 megapixels.

As particle detachment occurs throughout the experiment, the fraction of black pixels in the images varies with time. Therefore, the detachment fraction during a time step Δt can be determined as the relative change in black pixel fraction from time t to $t + \Delta t$ as presented in Eq. (10):

$$D_F = \frac{F_B(t) - F_B(t + \Delta t)}{F_B(t)} \quad (10)$$

CHAPTER IV

RESULTS AND DISCUSSION

A. Experimental Validation

Square flows alternating between blowing and suction were considered to test for resuspension under the effect of flow velocity, flow frequency and particle diameter. The purpose of the experiments is to validate the obtained numerical-analytical coupled results of the model [22] under the effect of square periodic flows.

To examine the flow profiles under which experiments were conducted, the flow meter (TSI 41211) mounted at the outlet of the tube of the “Periodic Flow Generating System” was used to track the flow response. Measurements of the profile were taken at the low and high flow velocities of 1.5 m/s and 3.5 m/s at frequencies of 0.5Hz and 0.25Hz each. All measured flows exhibited profiles similar to the experimental flow profile presented in **Fig. 5** at a velocity of 3.5m/s and a frequency of 0.5Hz. A transitional time of 0.05s was found between the blowing and suction phases due to the delay in the response of the valves. To apply similar flow conditions in the UDF of the CFD simulations, a short response time of linear acceleration was assumed for the flow at the first and last 0.05 s of each blowing and suction cycles, where the theoretical flow profile at a velocity of 3.5m/s and a frequency of 0.5Hz is also presented in **Fig. 5**.

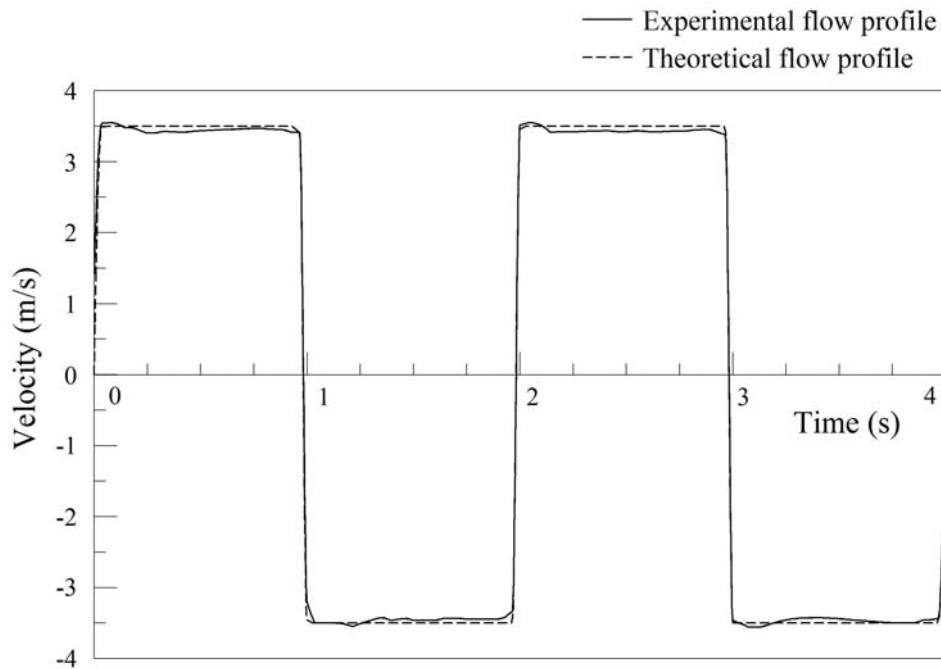


Figure 5: Experimentally measured flow profile compared to the theoretical flow profile

Following the proposed numerical methodology, CFD simulations were conducted to obtain the shear stress map generated under the effect of the square flows. Numerical simulations were carried under the conditions of the experimental setup. **Fig. 6** illustrates the mesh treatment used in the CFD simulations. Grid independence tests rendered a total of 438,300 elements with an element size of 0.5mm and five inflation layers over the sample test surface to measure accurate shear stress values. The first layer thickness was adjusted for each flow velocity to ensure obtaining y^+ values within the acceptable range. A time step of 0.0025s was used through the simulations to make sure convergence is attained with a scaled residual of 10^{-5} .

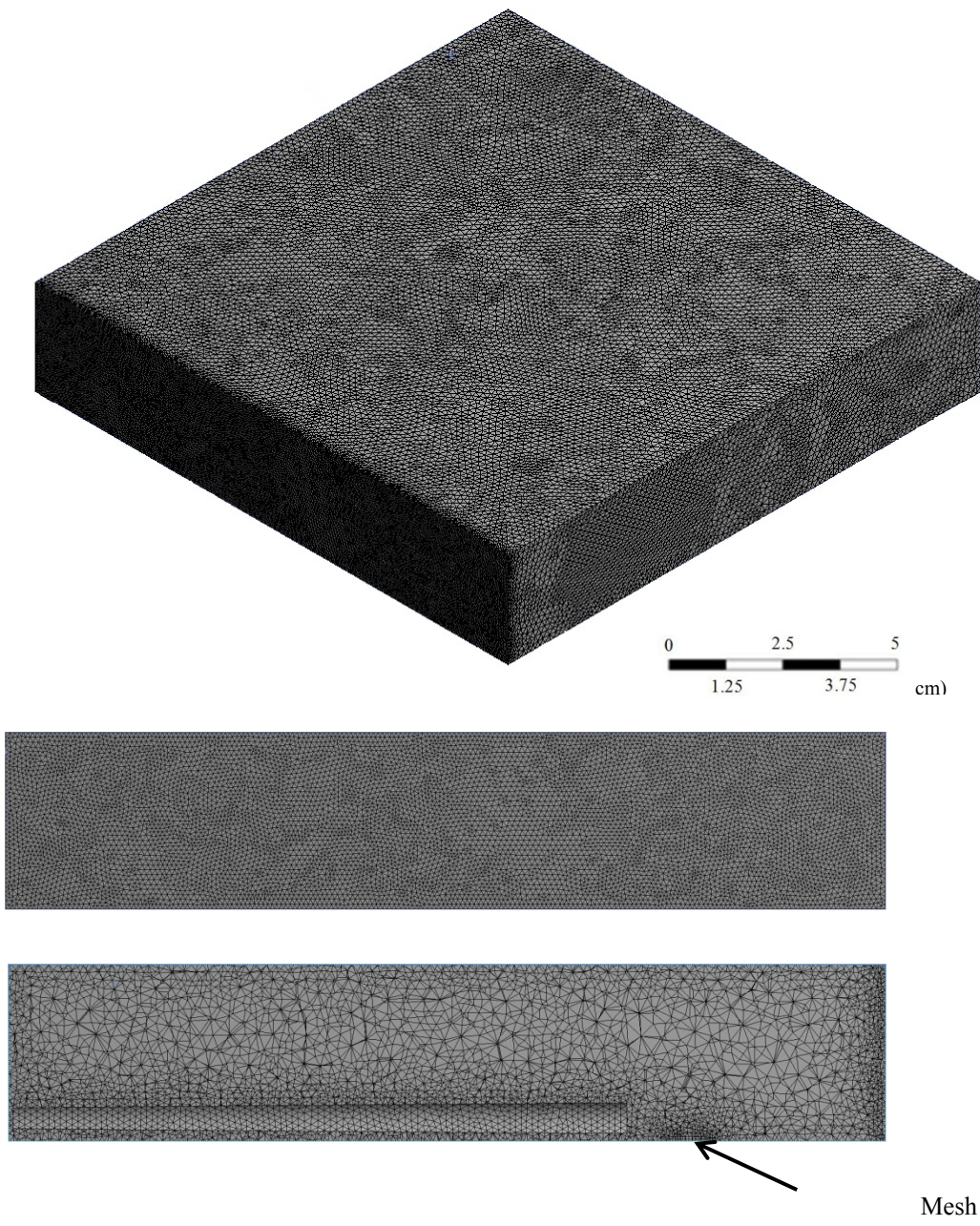


Figure 6: CFD mesh treatment: (a) 3D view (b) Frontal view and (c) Cross-sectional side view

Shear stress maps of the region surrounding the flow outlet for flow velocities of 1.5 m/s, 2.5m/s and 3.5m/s were obtained, where it was observed that the most

influenced area by the flow was located within a distance of 1cm from the flow outlet.

Fig. 7 represents the shear stress variations over the surface of interest examined at a flow velocity of 3.5m/s. Detachment fractions are computed within the maximum influence zone observed in the CFD simulations in a $1\text{ mm} \times 1\text{ mm}$ region located at a distance of 1cm from center of the flow outlet in which variations of shear stresses are minimal. This region is the same scan area observed under the microscope and considered for quantifying experimental detachment particle.

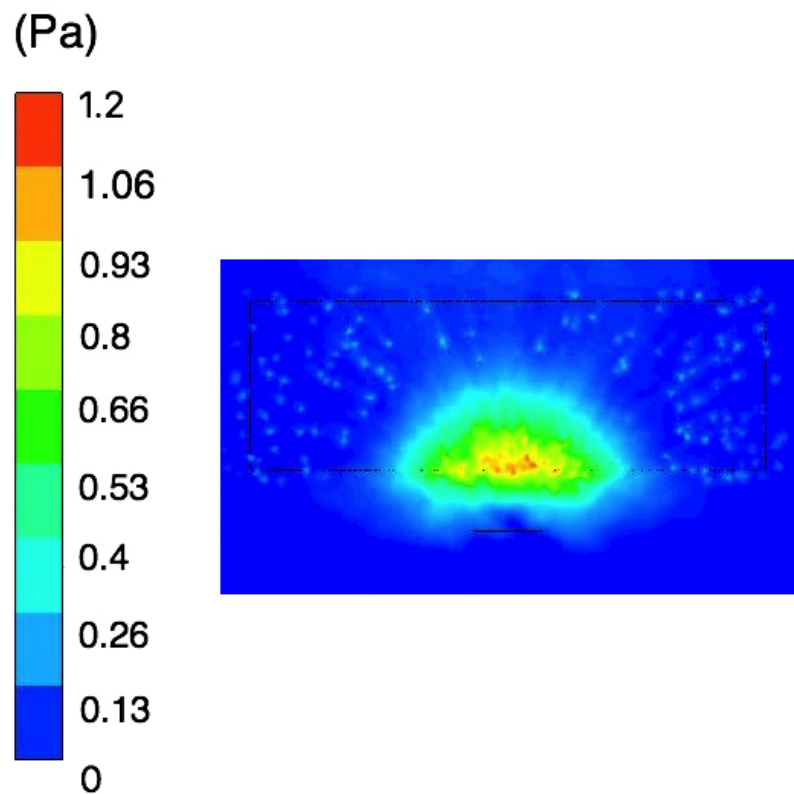


Figure 7: Shear stress variations over the region surrounding the flow outlet

Experimental validation was conducted to study the effect of the flow velocity, flow frequency and particle diameter on detachment fractions of polyethylene particles.

The experiments were repeated for a total of 6 times for each particle diameter of $49\mu\text{m}$ and $82.5\mu\text{m}$ at the three considered flow velocities of 1.5m/s, 2.5m/s and 3.5m/s and for frequencies of 0.5Hz and 0.25Hz. Snapshots at a rate of 5 per second were taken throughout the cycles of the square flow, where detachment fractions were measured and plotted as a function of the number of cycles at each flow velocity for both frequencies of 0.5Hz and 0.25Hz. Numerical simulations were conducted at the considered flow velocities and frequencies, where the obtained shear stresses were coupled with the analytical model to predict detachment fractions. . **Fig. 8(a)** and **Fig. 8(b)** present a comparison between the experimental and model results detachment fractions as a function of flow cycles for $49\mu\text{m}$ particles at both frequencies of 0.5Hz and 0.25Hz for flow velocities of 2.5m/s and 3.5m/s respectively. On the other hand, **Fig. 9(a-c)** presents the experimental and model results of detachment fractions as a function of flow cycles for $82.5\mu\text{m}$ particles at 0.5Hz and 0.25Hz for flow velocities of 1.5 m/s, 2.5 m/s and 3.5 m/s respectively. A good agreement was found between the experimentally measured detachment fractions and the numerical-analytical model predictions.

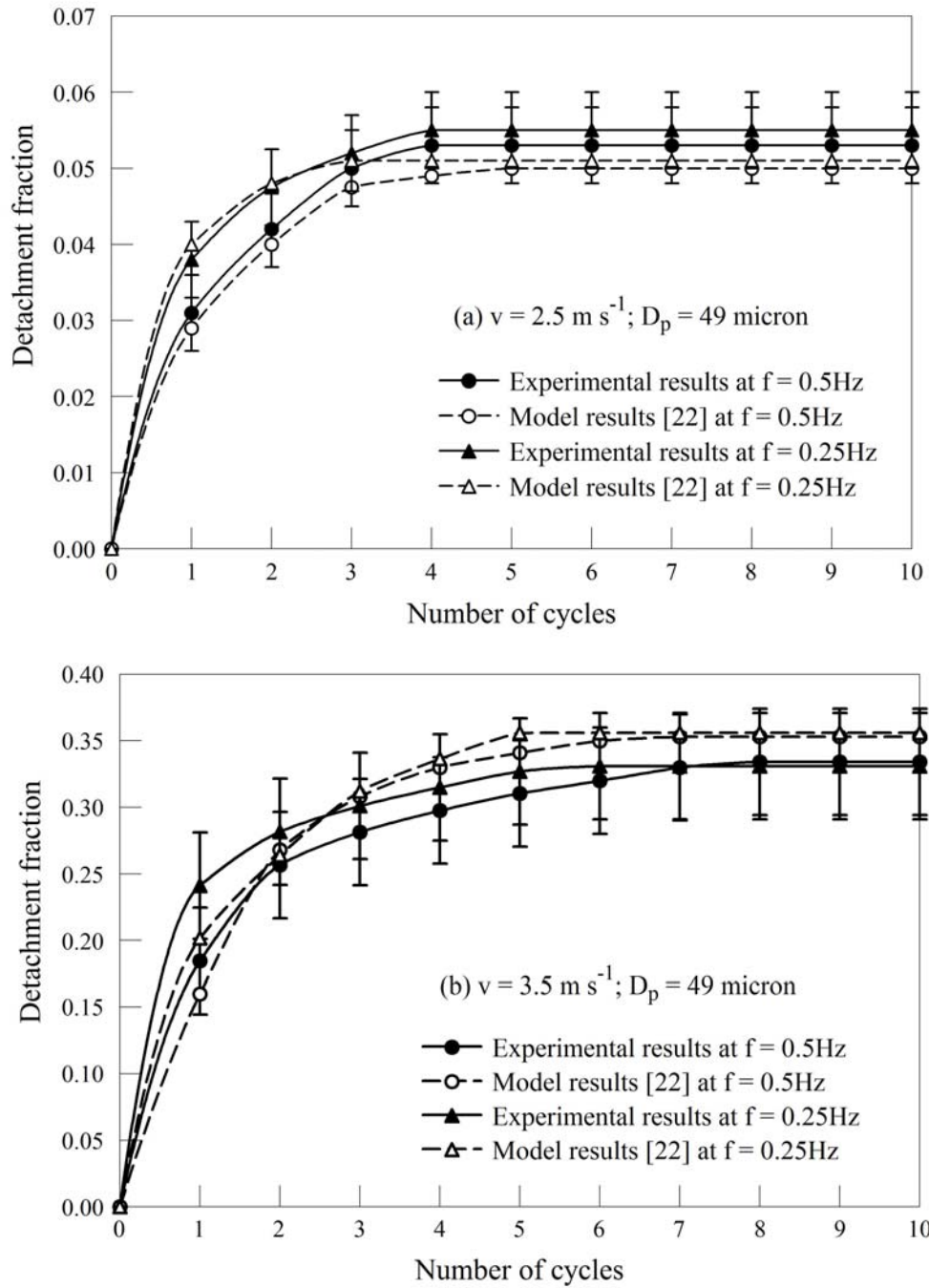


Figure 8: Detachment fraction variations for particles of $49 \mu\text{m}$ at flow frequencies of 0.5Hz and 0.25Hz for flow velocities of (a) 2.5m/s (b) 3.5m/s

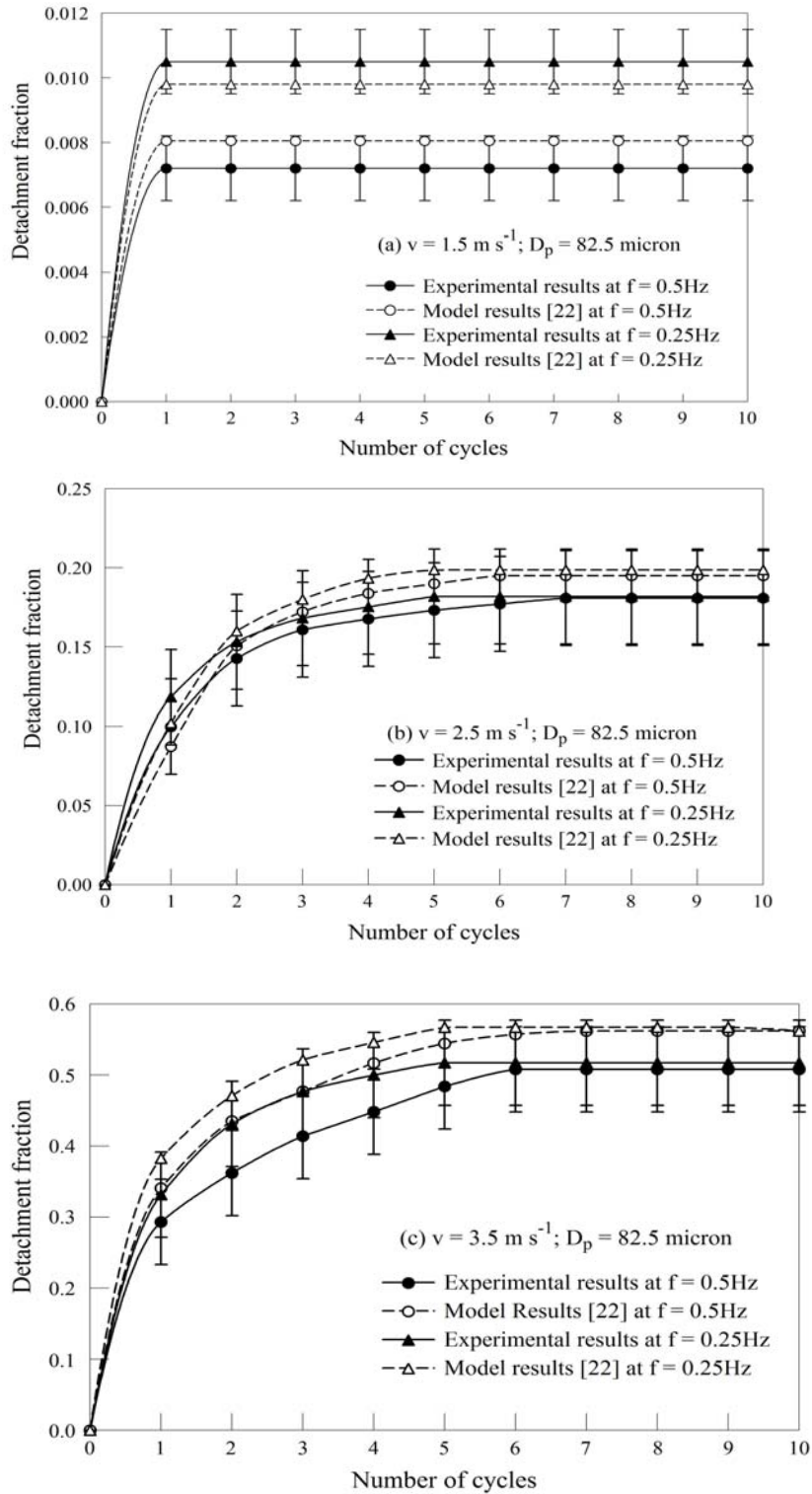


Figure 9: Detachment fraction variations for particles of $82.5\mu\text{m}$ at flow frequencies of 0.5Hz and 0.25Hz for flow velocities of (a) 1.5m/s (b) 2.5m/s (c) 3.5m/s

A significant fraction of particles was found to resuspend during the first cycle of the periodic flow, where the first cycle was the most influential cycle on the total detachment fraction. While at least 54% of the final detachment fraction of 49 μm particles resuspended during the first cycle at 3.5 m/s and 0.5Hz, approximately all particles of the final detachment fraction were observed to resuspend through the first cycle for 82.5 μm particles at 1.5m/s at both 0.5Hz and 0.25Hz. Moreover, a discharge phase was found to have a more significant effect on the total detachment throughout the periodic flow cycles being responsible of the majority of the resuspended fraction during a single cycle. At a flow velocity of 1.5 m/s and a frequency of 0.5Hz, a discharge cycle was responsible of resuspending 62% of 82.5 μm particles compared to a 38% during a suction cycle. On the other hand, at a flow velocity of 3.5 m/s and a frequency of 0.5Hz, the detachment fraction during the discharge phase was responsible for around 92% of the detachment fraction of 49 μm polyethylene particles throughout a cycle compared to an 8% during a suction phase. This agrees with the shear stress values computed over the surface at a flow velocity of 3.5 m/s and a frequency of 0.5Hz, where values were found to be around 3.5 times higher during a blowing phase of the cycles compared to shear stress values during a suction cycle as shown in **Fig. 10**.

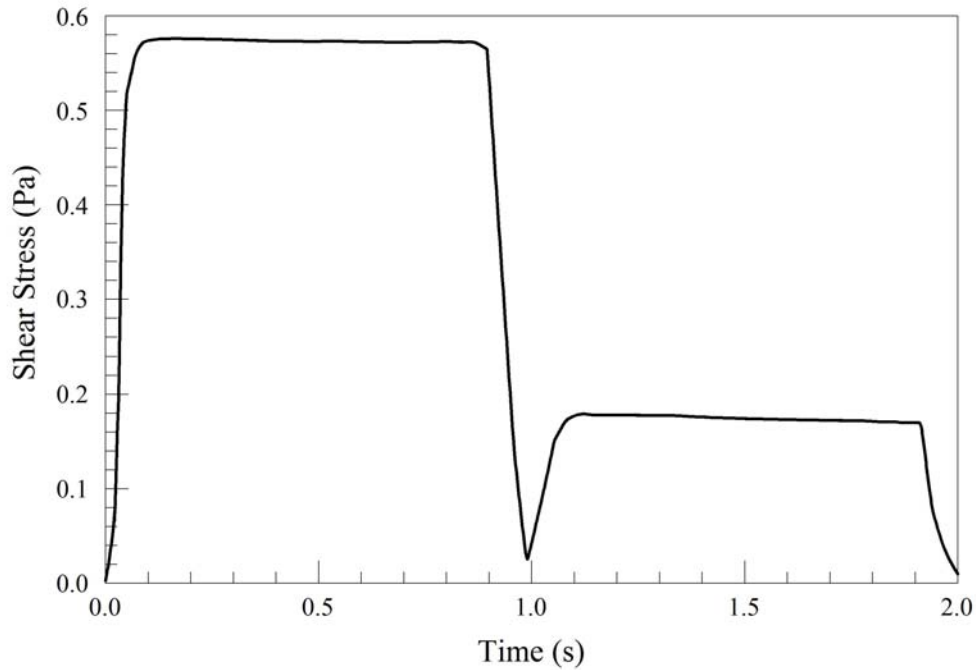


Figure 10: Shear stresses during a blowing phase between 0 and 1s and a suction phase between 1 and 2s

It is observed that as the flow cycles progress, the rate of detachment fractions decreases. The locations of occurrence of turbulent bursts differ from one cycle to another as they follow a normal Gaussian profile. Thus as the number of cycles increases no resuspension will occur over the locations covered by threshold turbulent bursts in previous cycles over-which particles have already resuspended. On the other hand, particles over new locations where no threshold turbulent bursts have previously taken place will resuspend in case of a burst occurrence in these locations. As the cycles progress, the number of locations not covered by threshold burst occurrence decreases causing reduced detachment fractions to occur which justifies the decrease in the rate of detachment fractions with the increase in the number of cycles.

Considering polyethylene particles of size $49\mu\text{m}$ and at a flow frequency of 0.5Hz, no resuspension was observed at a velocity of 1.5m/s, however; higher final detachment percentages of 5.2% and 33.1% were measured at increasing velocities of 2.5m/s and 3.5m/s respectively as shown in **Fig. 8(a)** and **Fig. 8(b)**. This can be justified by higher shear values generated over the surfaces as the velocity of the periodic flow is increased. With a maximum relative experimental error of 10% measured for the samples at the three velocities, the model was able to estimate detachment fractions with a relative error in order of 8% for flow a flow velocity of 1.5m/s, and in the order of 10% for flow velocities of 2.5m/s and 3.5m/s.

At a frequency of $f=0.25\text{Hz}$, the total resuspension fraction converged to a final value within a fewer number of cycle compared to a higher frequency of $f=0.5\text{Hz}$ at both flow velocities of 2.5m/s and 3.5m/s for a particle size of $49\mu\text{m}$. However, at each of the flow velocities, the final resuspension fraction reached at a frequency of $f=0.25\text{Hz}$ was the same as the fraction reached at a frequency of $f=0.5\text{Hz}$. For a flow velocity of 3.5 m/s and a frequency of $f=0.25\text{Hz}$, the final detachment fraction was attained within 5 cycles of square flows, while at a frequency of $f=0.5\text{Hz}$ the final fraction of resuspension was attained within 7 cycles. The model was able to predict the number of cycles to reach a steady resuspension fraction with an error of prediction of ± 1 cycle.

Experimental validation to examine the effect of particle diameter was conducted at a particle diameter of $82.5\mu\text{m}$ at velocities of 1.5m/s, 2.5m/s and 3.5m/s for both frequencies of 0.5Hz and 0.25Hz. Experimental results have shown higher detachment fraction at a particle diameter of $82.5\mu\text{m}$ compared to detachment fractions at a particle diameter of $49\mu\text{m}$ as shown in **Fig. 9(a-c)**. While no resuspension was

observed at a velocity of 1.5m/s for 49 μm particles at 0.25Hz, a total of approximately 1% of the 82.5 μm resuspended at same velocity and frequency. On the other hand, a total of 51.8% of the particles resuspended at 3.5m/s at 0.25Hz compared to 33.1% for 49 μm particles at the same conditions. Resuspension fractions increase with particle diameter since the ratio of removal to adhesive moments and forces increases [23]. The maximum experimental relative error was 8.5% for 82.5 μm particles at the three velocities where the model was able to capture the effect of particle diameter on resuspension under oscillatory flows with a relative error of 10%.

B. Parametric Study

To examine the applicability of the validated model [22] under oscillatory flows, a parametric study of realistic physical cases is conducted to test for micro-particle detachment from indoor surfaces under human respiration. In several situations, breathing may take place close to a surface seeded with particles such as during sleeping, praying positions and crawling infants on floors, thus posing a risk of resuspension and inhalation of these particles [19]. The aim of this study is to assess the capability of the human respiration in initiating the detachment of a selection of particle types from a variety of flooring materials at several proximities from the human nostril. The same setup of the experimental validation section is used to conduct the parametric study however; detachment fractions are measured at several distances from the flow outlet. Sinusoidal flow profiles were chosen to model respiratory activities since the flow pattern of a human breathing is nearly sinusoidal [20], which is similar to the profile presented previously and shown at the bottom left of **Fig. 1(c)**. The sinusoidal flow velocity is defined in the UDF and is given by Eq. (11):

$$v(t) = V_{s,max} \sin(2\pi ft) \quad (11)$$

where, $V_{s,max}$ is the maximum velocity of the sinusoidal flow, f is the flow frequency and t is the time. A breathing frequency of 0.23Hz was taken for normal respiration with a maximum flow velocity of 4.3 m/s, assuming the body is in a resting position [20]. The maximum flow velocity from the nose was calculated based on an average flow rate for inhalation and exhalation computed by Habchi et al. [20] given in Eq. (12) assuming a nasal opening area of 0.91 cm^2 [31]:

$$q_{avg}(t) = 3.9 \times 10^{-3} \sin(1.445t) \quad (12)$$

The same profile was taken for respiration in a laying position, where breathing is taking place close to a surface with dust particles. The geometry of the setup is kept the same throughout the study. Particle characteristics (particle diameter and type) and the flooring material are varied distinctively to examine the effect of each on resuspension under the influence of normal respiration, while keeping the others fixed. The final detachment fraction is evaluated at 10 circular points of diameter 1mm in which no significant shear stress variations are observed within. The points fall on a 25mm vertical line lying on the center of the flow outlet, where the points are placed at intervals of 2.5mm within the shear stress influence zone of breathing as shown in **Fig. 11**. Table 2. presents the set of parameters along with their selections throughout the study. The study includes testing for detachment under four flooring materials (ceramic, rough ceramic, marble and parquet) which have been identified to be commonly used in indoor spaces [35]. On the other hand, resuspension is examined under two particle types (lead and nickel) which were previously recognized as abundant dust particles present in houses and two particle diameters of $25 \mu\text{m}$ and $80 \mu\text{m}$ with a 10% variation in diameter falling within the range of human exposure risk

assessment [7,8, 36]. Both flooring materials and particle types have their properties and characteristics available and presented in Tables 3 and 4 [37].

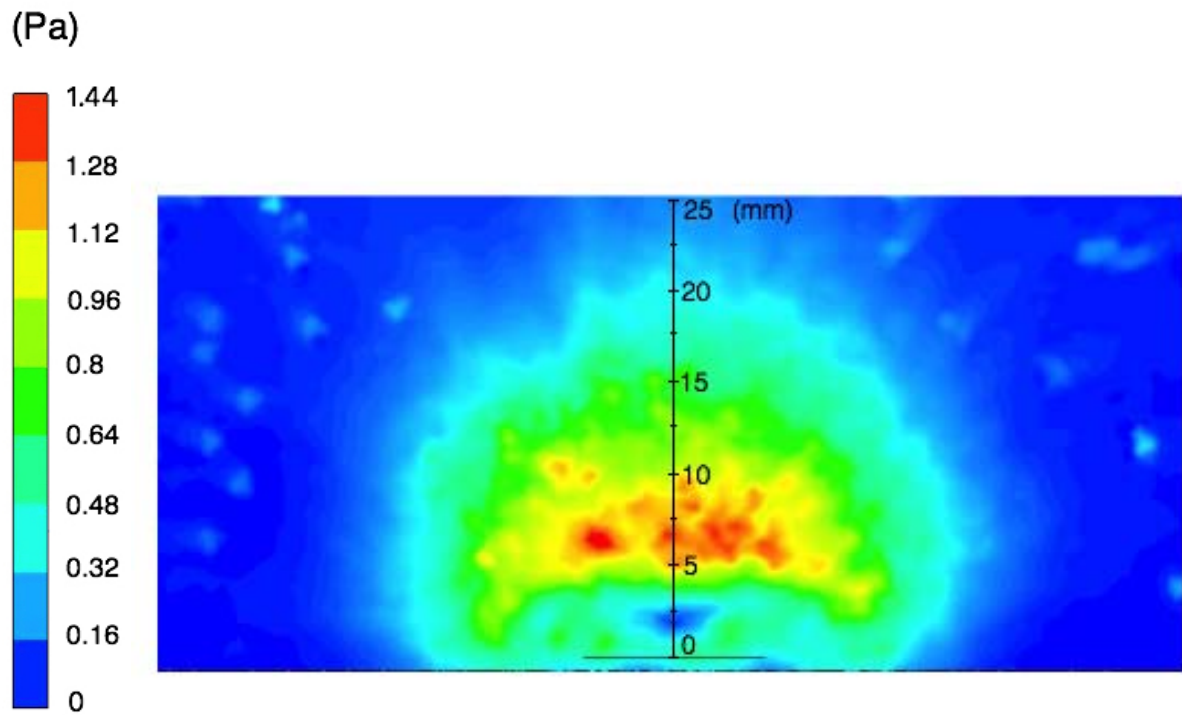


Figure 11: Shear stress variation over the surface under the influence of normal breathing

Table 2: Boundary conditions used for the setup in the parametric study

Parameter	Range/Value
Plexiglas Box Dimensions	0.2m long; 0.2m wide; 0.04 height
Range of distances of substrate from outlet of the tube	[0; 0.025m]
Airflow Profile	Sinusoidal
Maximum Airflow Velocity	4.28m/s
Airflow Frequency	0.23Hz
Substrate – Flooring Materials	Ceramic/Marble/Parquet
Particles’ Material	Lead/Nickel
Average Particle Diameter Range	[25μm, 80 μm]
Range of Average Roughness of Flooring Material	[0.96μm – 14.54μm]

Table 3: Particle properties used in the parametric study

Particle Material	Lead	Nickel
Particle Density	11340 kg/m³	8908 kg/m³
Poisson’s Ratio	0.42	0.31
Surface Energy of Material	442 mJ/m²	1770 mJ/m²
Young’s Modulus of Material	13.789 GPa	200GPa

Table 4: Substrate / Flooring properties used in the parametric study

Substrate Material	Smooth Ceramic	Rough Ceramic	Parquet	Marble
Density of Material	3223 kg/m ³	3223 kg/m ³	461 kg/m ³	2790.4 kg/m³
Average Surface Roughness	3.39μm	14.54μm	4μm	0.96μm
Surface Energy of Material	560 mJ/m²	560 mJ/m²	50 mJ/m²	865 mJ/m²
Poisson’s Ratio of Material	0.22	0.22	0.408	0.25
Young’s Modulus of Material	50GPa	50GPa	9GPa	756Pa

Marble tiles being a commonly used flooring material in indoor spaces is considered to examine the detachment of lead and nickel particles of both diameters $25\ \mu\text{m}$ and $80\ \mu\text{m}$ under the influence of human breathing. **Fig. 12(a)** and **Fig. 12(b)** show the final resuspension fraction for lead and nickel particles respectively of the two considered particle sizes observed at different distances from the flow outlet. Two distinct regions can be identified over the surface leading to a variation in the detachment fractions with the distance from the flow outlet. Moving away from the flow outlet, it was observed that the shear stresses generated by the respiratory flow increased with distance after which the surface experienced a location of maximum of shear stresses as shown in **Fig. 11**. Following this increase in shear stresses, the weakened flow by the entrainment of surrounding air causes a decrease in the shear stresses as the flow moves further over the surface. The variations in the shear stresses with distance from the flow outlet justify the increase followed by the decrease in detachment fractions observed as a function of distance from the flow outlet as shown in **Fig. 12(a)** and **Fig. 12(b)**.

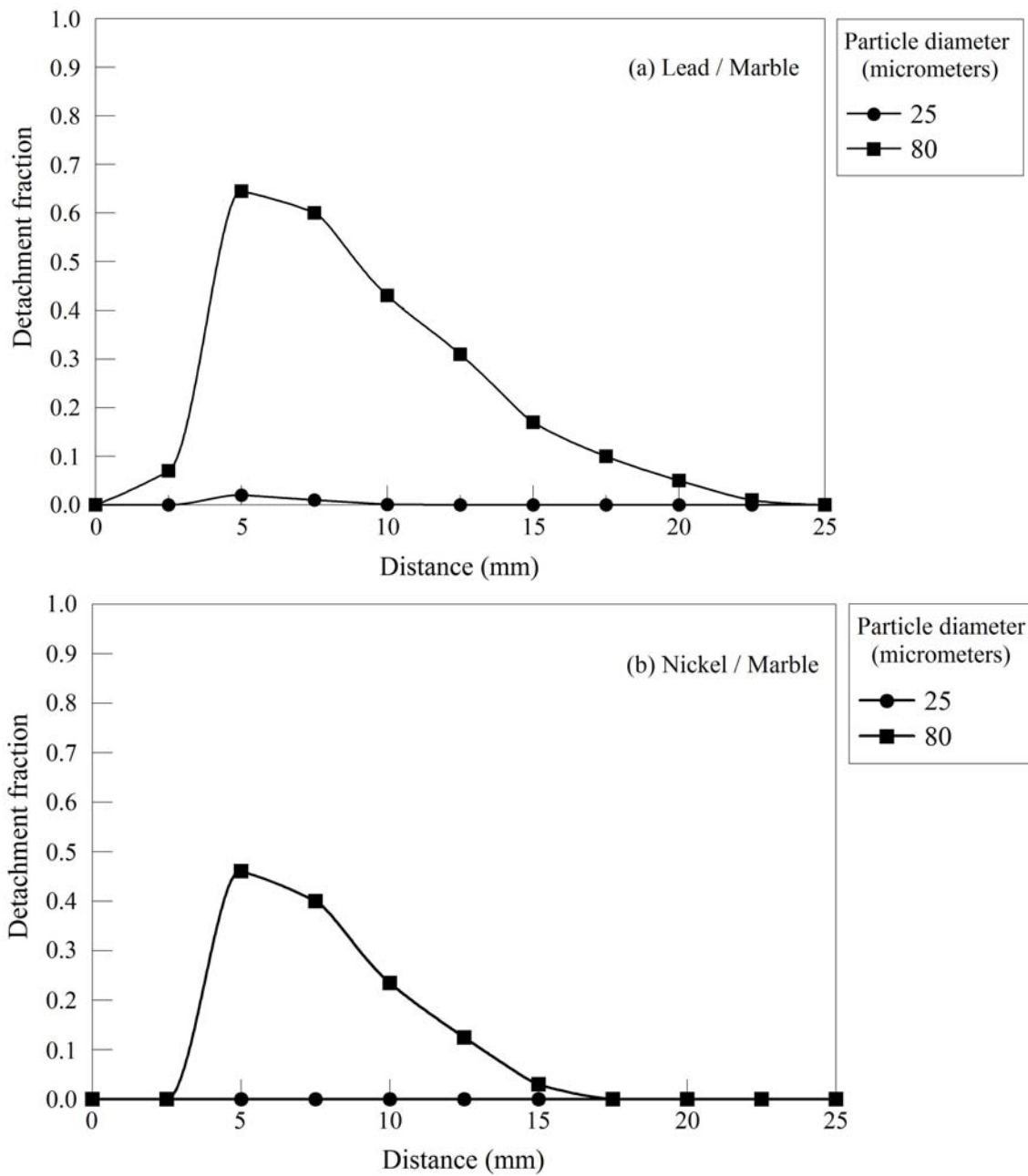


Figure 12: Detachment fraction variations for (a) lead (b) nickel particles of sizes 25 μm and 80 μm

Increasing detachment fractions were obtained with increasing particle diameters, where a maximum detachment of 64.5% occurred for lead particles of size

80 μm at a distance of 5mm, where the highest shear stresses were recorded as shown in **Fig. 12(a)**. On the other hand, a detachment of 2.8% occurred for lead particles of size 25 μm at the same location of maximum shear stresses. The ratio of removal to adhesive moments and forces increases with larger particle diameters causing higher detachment fractions to occur [22]. Thus particles of increasing diameters pose a higher risk of resuspending compared to those of smaller sizes present in indoor spaces. A similar behavior was examined for nickel particles having a particle diameter of 80 μm , where a maximum detachment of 46.1% was recorded at a distance of 5mm from the flow outlet, however no resuspension was observed for nickel particles of size 25 μm at all locations of the flow influence zone as presented in **Fig. 12(b)**. The higher detachment fractions of lead particles compared to the fractions for nickel particles can be justified by the significant influence of a particle's surface energy on the occurrence of resuspension. The surface energy of a particle contributes to the adhesive force between the particle and the surface, thus lower detachment fractions occur for particles possessing higher surface energies [22]. The detachment fractions were observed higher for lead particles as it has a relatively lower surface energy compared to nickel particles.

The floor type is varied between four selections of smooth ceramic, rough ceramic, parquet and marble to examine the resuspension of lead and nickel particles of diameter 80 μm at several distances under the influence normal breathing. The only difference between rough and smooth ceramic is in the surface roughness of the material, while all other flooring materials differ in both their surface roughness and surface energy, which are both influential on the occurrence of detachment [22].

Fig. 13(a) and **Fig 13(b)** present the final resuspension fractions of lead and nickel particles respectively under the four considered floor types at different distances from

the flow outlet. As the surface roughness of the flooring surface increases higher resuspension is expected to occur which can be observed over rough ceramic surfaces compared to smooth ceramic flooring material. A maximum detachment of 92.1% occurred for lead particles over rough ceramic at the point of highest shear stresses at 5mm compared to a maximum of 77.8% for lead particles under smooth ceramic at the same point as shown in **Fig. 13(a)**. On the other hand, detachment fractions decrease with higher surface energies of the substrate material. Higher surface energy and lower roughness of the flooring material contribute to increasing adhesive forces between the surface and particle, thus decreasing the chances of resuspension occurrence [22]. For this reason, a significantly higher resuspension fraction of 98.3% was measured for lead particles over parquet flooring at a distance of 5mm, which is due to the relatively low surface energy and higher roughness of parquet compared to that of ceramic and marble. A similar behavior was examined for nickel particles where the highest resuspension was recorded over a parquet floor with a maximum of 81% while the lowest resuspension occurred over marble with a maximum of 46.1%.

The study has shown that resuspension can occur under normal breathing close to a surface carrying different dust micro particles. Detachment of particles with relatively large sizes is more likely to occur than relatively small particles, thus more attention should be paid to larger particles in indoor spaces and to the methods of their removal. On the other hand, the choice of the flooring material can help in hindering the occurrence of detachment. Through the parametric study, it has been noted that resuspension is more likely to occur over parquet flooring compared to other flooring materials therefore, it is preferable to replace parquet with other flooring materials as marble, which is considered a safer material and might reduce resuspension.

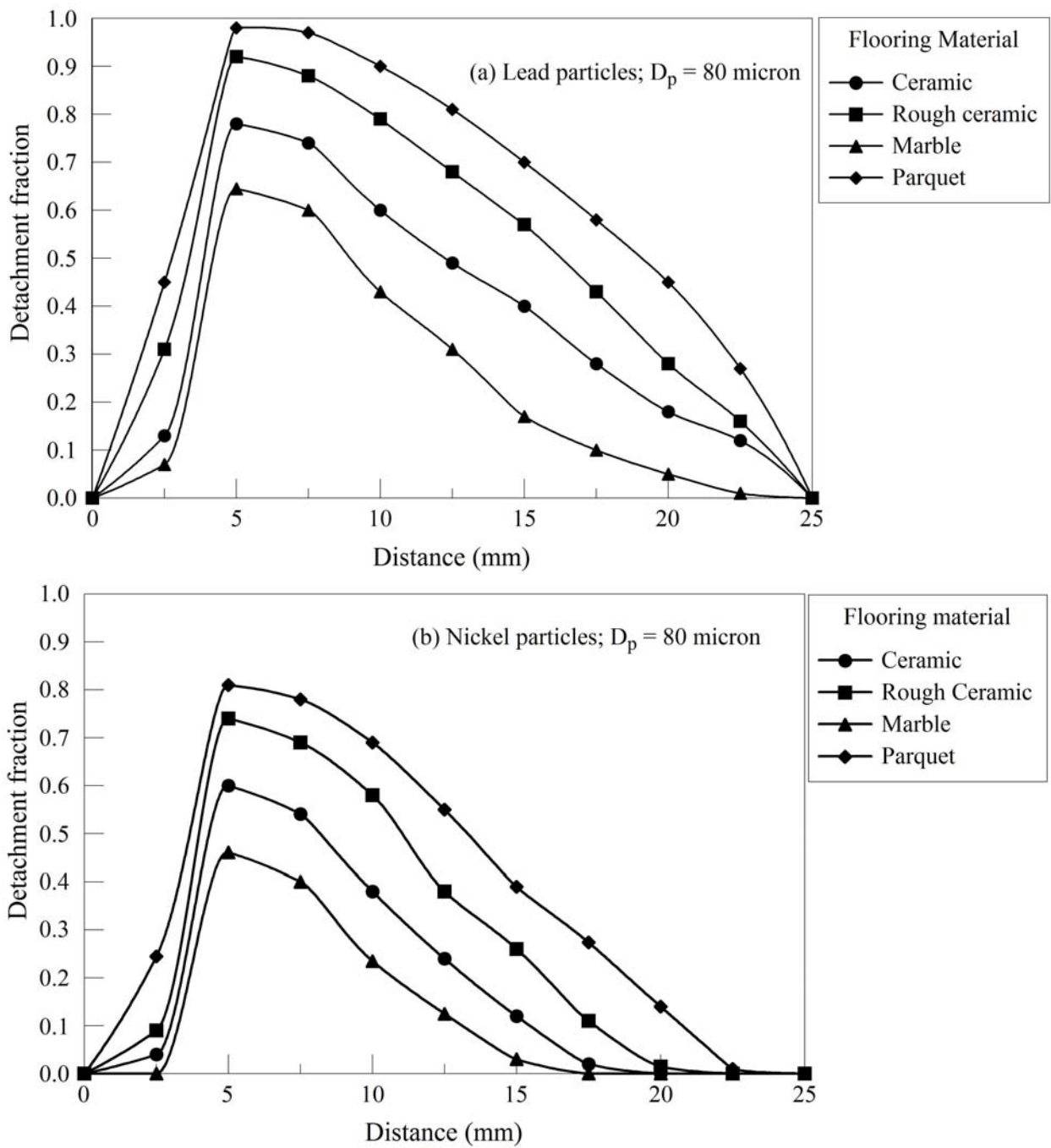


Figure 13: Detachment fraction variations for (a) lead and (b) nickel particles of size $80\mu\text{m}$ under different flooring materials

CHAPTER VI

CONCLUSION

Experimental and numerical-analytical work is conducted to validate and apply a developed resuspension transient model under periodic flows. Experimental validation of the model included testing for the effect of the flow velocity, frequency and the particle diameter under generated periodic square flows, where detachment fractions were monitored over the cycles of the flow. The obtained resuspension fractions were found to be in good agreement with the model predictions with a relative error in the order of 10%. The validated model was used to conduct a parametric study investigating particle detachment under respiration where a human is breathing close to a surface carrying dust particles.

Different particle characteristics and flooring materials were considered under normal breathing of a human being. Final resuspension fractions showed that resuspension for particles with relatively large diameters is higher than the detachment occurrence for smaller sized particles. On the other hand, detachment is more likely to occur for particles with low surface energies and over flooring materials of low surface energy and high surface roughness, which are properties that facilitate resuspension occurrence. It was observed that parquet highly influences particle detachment, so choosing safer materials such as marble and smooth ceramic can reduce the chances indoor resuspension. Keeping in mind that the flooring material can be chosen to reduce resuspension occurrence and breathing close to surfaces can be avoided, it would be

interesting to consider in future work the capability of air ventilation systems in reducing indoor concentrations of particles of different types and sizes.

In conclusion, the transient resuspension model has proven to be capable of predicting resuspension under periodic flows with different physical characteristics, thus the model can be applied to future work involving all kinds of natural periodic flows.

BIBLIOGRAPHY

- [1] Loosmore, G. A. (2003). Evaluation and development of models for resuspension of aerosols at short times after deposition. *Atmospheric environment*, 37(5), 639-647.
- [2] Brodsky, A. L. L. E. N. (1980). Resuspension factors and probabilities of intake of material in process (or 'Is 10⁻⁶ a magic number in health physics'). *Health Physics*, 39(6), 992-1000.
- [3] Ozkaynak, H., Xue, J. S. J. W. L. P. E. J. P., Spengler, J., Wallace, L., Pellizzari, E., & Jenkins, P. (1995). Personal exposure to airborne particles and metals: results from the Particle TEAM study in Riverside, California. *Journal of Exposure Analysis and Environmental Epidemiology*, 6(1), 57-78.
- [4] Abt, E., Suh, H. H., Catalano, P., & Koutrakis, P. (2000). Relative contribution of outdoor and indoor particle sources to indoor concentrations. *Environmental science & technology*, 34(17), 3579-3587.
- [5] Roberts, J. W., Budd, W. T., Ruby, M. G., Camann, D. E., Fortmann, R. C., Lewis, R. G., ... & Spittler, T. M. (1992). Human exposure to pollutants in the floor dust of homes and offices. *J Expo Anal Environ Epidemiol*, 2(Suppl 1), 127-146.
- [6] Rasmussen, P. E., Levesque, C., Chénier, M., Gardner, H. D., Jones-Otazo, H., & Petrovic, S. (2013). Canadian House Dust Study: Population-based concentrations, loads and loading rates of arsenic, cadmium, chromium, copper, nickel, lead, and zinc inside urban homes. *Science of the Total Environment*, 443, 520-529.
- [7] Wallace, L. (2006). Indoor sources of ultrafine and accumulation mode particles: size distributions, size-resolved concentrations, and source strengths. *Aerosol science and technology*, 40(5), 348-360.
- [8] Kuo, C. Y., Wang, J. Y., Liu, W. T., Lin, P. Y., Tsai, C. T., & Cheng, M. T. (2012). Evaluation of the vehicle contributions of metals to indoor environments. *Journal of Exposure Science and Environmental Epidemiology*, 22(5), 489-495.
- [9] Rasmussen, P. E., Subramanian, K. S., & Jessiman, B. J. (2001). A multi-element profile of house dust in relation to exterior dust and soils in the city of Ottawa, Canada. *Science of the Total Environment*, 267(1), 125-140.

- [10] Cao, Z. G., Yu, G., Chen, Y. S., Cao, Q. M., Fiedler, H., Deng, S. B., ... & Wang, B. (2012). Particle size: a missing factor in risk assessment of human exposure to toxic chemicals in settled indoor dust. *Environment international*, 49, 24-30.
- [11] Sporik, R., PLATTS-MILLS, T. A. E., & Cogswell, J. J. (1993). Exposure to house dust mite allergen of children admitted to hospital with asthma. *Clinical & Experimental Allergy*, 23(9), 740-746.
- [12] Sehmel, G. A. (1980). Particle resuspension: a review. *Environment International*, 4(2), 107-127.
- [13] Thatcher, T. L., & Layton, D. W. (1995). Deposition, resuspension, and penetration of particles within a residence. *Atmospheric Environment*, 29(13), 1487-1497.
- [14] Lai, A. C., Thatcher, T. L., & Nazaroff, W. W. (2000). Inhalation transfer factors for air pollution health risk assessment. *Journal of the Air & Waste Management Association*, 50(9), 1688-1699.
- [15] Raja, S., Xu, Y., Ferro, A. R., Jaques, P. A., & Hopke, P. K. (2010). Resuspension of indoor aeroallergens and relationship to lung inflammation in asthmatic children. *Environment international*, 36(1), 8-14.
- [16] Sears, M. R., Herbison, G. P., Holdaway, M. D., Hewitt, C. J., FLANNERY, E. M., & Silva, P. A. (1989). The relative risks of sensitivity to grass pollen, house dust mite and cat dander in the development of childhood asthma. *Clinical & Experimental Allergy*, 19(4), 419-424.
- [17] Miguel, A. G., Cass, G. R., Glovsky, M. M., & Weiss, J. (1999). Allergens in paved road dust and airborne particles. *Environmental science & technology*, 33(23), 4159-4168.
- [19] Qian, J., & Ferro, A. R. (2008). Resuspension of dust particles in a chamber and associated environmental factors. *Aerosol Science and Technology*, 42(7), 566-578.
- [20] Habchi, C., Ghali, K., & Ghaddar, N. (2014). Improved thermal performance of face mask using phase change material. *Textile Research Journal*, 84(8), 854-870.
- [21] Reeks, M. W., Reed, J., & Hall, D. (1988). On the resuspension of small particles by a turbulent flow. *Journal of Physics D: Applied Physics*, 21(4), 574.

- [22] Habchi, C., Ghali, K., & Ghaddar, N. (2016). Coupling CFD and analytical modeling for investigation of monolayer particle resuspension by transient flows. *Building and Environment*, 105, 1-12.
- [23] Ibrahim, A. H., Dunn, P. F., & Brach, R. M. (2003). Microparticle detachment from surfaces exposed to turbulent air flow: controlled experiments and modeling. *Journal of aerosol science*, 34(6), 765-782.
- [24] Menon, A. S., Weber, M. E., & Chang, H. K. (1984). Model study of flow dynamics in human central airways. Part III: Oscillatory velocity profiles. *Respiration physiology*, 55(2), 255-275.
- [25] ANSYS Software: ANSYS Inc. <http://www.ansys.com/>.
- [26] MATLAB Software: Math Works Inc. <http://www.mathworks.com/products/matlab/>
- [27] Soltani, M., & Ahmadi, G. (1994). On particle adhesion and removal mechanisms in turbulent flows. *Journal of Adhesion Science and Technology*, 8(7), 763-785.
- [28] Saffman, P. G. T. (1965). The lift on a small sphere in a slow shear flow. *Journal of fluid mechanics*, 22(02), 385-400.
- [29] A.H. Ibrahim, P.F. Dunn, R.M. Brach, Microparticle detachment from surfaces exposed to turbulent airflow: controlled experiments and modeling, *J. AerosolSci.* 34 (2003) 765–782.
- [30] K.L. Johnson, K. Kendall, A. Roberts, Surface energy and contact of elastic solids, *Proc. R. Soc. A* 324 (1971) 301–313.
- [31] Mohebbi, A., Farhadi, M., & Erfan, A. (2008). Assessment of nasal volume and cross-sectional area by acoustic rhinometry in a sample of normal adult Iranians. *Arch Iran Med*, 11(5), 555-8.
- [32] Murakami, S. (2004). Analysis and design of micro - climate around the human body with respiration by CFD. *Indoor Air*, 14(s7), 144-156.
- [33] Klinger, T. (2003). *Image processing with LabVIEW and IMAQ Vision*. Prentice Hall Professional.
- [34] Liao, C. W., Yu, J. H., & Tarng, Y. S. (2010). On-line full scan inspection of particle size and shape using digital image processing. *Particuology*, 8(3), 286-292.

- [35] Lloyd, D. G. (1992). An Investigation of Floor Surface Profile Characteristics That Will Reduce the Incidence of Slips and Falls.
- [36] Adkins, B., Richards, J. H., & Gardner, D. E. (1979). Enhancement of experimental respiratory infection following nickel inhalation. *Environmental research*, 20(1), 33-42.
- [37] Kinloch, A. (2012). *Adhesion and adhesives: science and technology*. Springer Science & Business Media.
- [38] Abdullah, S. F., Saeed, S. A., & Qadir, S. S. (2015). Comparative Study of Terrazzo Tiles Produced in Koya and Erbil, and its Suitability for Construction Purposes. *ARO-THE SCIENTIFIC JOURNAL OF KOYA UNIVERSITY*, 3(2), 11-17.